

State-sensitive monitoring of gold nanoparticle sites on titania and the interaction of the positive Au site with O₂ by Au L_α₁-selecting X-ray absorption fine structure [☆]

Yasuo Izumi ^{a,*}, Daa Mosbah Obaid ^b, Kazushi Konishi ^b, Dilshad Masih ^b, Masafumi Takagaki ^c, Yasuko Terada ^c, Hajime Tanida ^c, Tomoya Uruga ^{c,*}

^a Graduate School of Science, Chiba University, Yayoi 1-33, Inage-ku, Chiba 263-8522, Japan

^b Interdisciplinary Graduate School of Science and Engineering, Tokyo Institute of Technology, Nagatsuta 4259, Midori-ku, Yokohama 226-8502, Japan

^c Japan Synchrotron Radiation Research Institute, Kohto 1-1-1, Sayo 679-5198, Japan

Received 17 April 2007; received in revised form 14 September 2007; accepted 16 September 2007

Available online 29 October 2007

Dedicated to Edward Solomon.

Abstract

The heterogeneity of gold sites in various Au/TiO₂ catalysts was studied by means of state-sensitive Au L₃-edge X-ray absorption fine structure (XAFS) combined with high energy-resolution X-ray fluorescence spectrometry. A series of Au/TiO₂ catalysts were prepared via deposition-precipitation method on anatase-type or mesoporous (amorphous) TiO₂ added with NaOH (lower Au loading) or urea (higher Au loading). The mean Au particle size ranged between 29 and 87 Å based on high-resolution TEM (transmission electron microscope) measurements. The Au L_α₁ emission peak energy for Au/mesoporous-TiO₂ in air and Au/anatase-TiO₂ in CO (5%) corresponded to Au⁰ state. The emission peak energy for Au/anatase-TiO₂ in air shifted toward that of Au^I state. For relatively greater Au particles (average 87 Å) dispersed on mesoporous TiO₂, the major valence state discriminated by Au L_α₁-selecting XANES (X-ray absorption near-edge structure) spectrum tuned to Au L_α₁ emission peak top was Au⁰, but the Au^{δ-} state could be successfully monitored by Au L_α₁-selecting XANES tuned to the emission energy at 9707.6 eV, of which population was relatively small compared to the case of smaller Au particles (average 29 Å) on anatase-type TiO₂. On the other hand, negative charge transfer from Au 5d to support was demonstrated in Au^{δ+}-state sensitive XANES tuned to 9718.3–9718.7 eV. The Au^{δ+}-state sensitive XANES spectra resembled theoretically generated XANES for interface Au^{δ+} sites model on TiO₂ in contact with surface Ti sites. Further charge transfer was demonstrated from Au to adsorbed O₂ for Au/anatase-TiO₂ catalyst.

© 2007 Elsevier B.V. All rights reserved.

Keywords: Gold; Titanium oxide; X-ray absorption fine structure; Fluorescence spectrometry; Chemical state

1. Introduction

Gold is chemically inert, however, it was found to become active when dispersed as nano-particles of size 30 Å or smaller in low temperature CO oxidation [1,2].

Various possibilities have been proposed as the active sites: anionic Au cluster site, perimeter site, and lower-coordination step-edge site [1,2]. However, it is difficult to observe each site one by one among Au nano-particles dispersed over porous, complex surface of TiO₂.

In order to overcome the heterogeneity problem of Au sites, we applied state-sensitive XAFS spectroscopy [3,4] to a series of Au/TiO₂ samples. Due to the differences of deposition-precipitation (DP) conditions of Au compound with NaOH or urea, reaction time of DP, and crystalline

[☆] Part 23 in the series.

* Corresponding authors. Tel./fax: +81 43 290 3696.

E-mail addresses: yizumi@faculty.chiba-u.jp (Y. Izumi), urugat@spring8.or.jp (T. Uruga).

phase of TiO₂ support (anatase/rutile or amorphous), particle size and loading amount of Au were systematically controlled. Catalytically active Au nano-particle sites populated in narrow size distribution centered at 29 Å were monitored state-sensitively in CO or O₂ atmosphere to extract activation sites for the low-temperature oxidation reaction.

In this spectroscopic method, better-resolved, steeper XANES spectra were obtained to remove the core-hole lifetime width (Γ) of K levels for Cu [4,5] and Sn [4] and L₃ levels for Dy [6], Pt [7], and Pb [4,8] by selecting the K α_1 and L α_1 emission, respectively.

2. Experimental

2.1. Samples

K⁺[Au^I(CN)₂]⁻ (Wako) was thoroughly mixed with boron nitride (BN) to be 1.0 wt% Au and pressed into a disk of 20 mm in diameter. Au metal foil was controlled to be the thickness of 6 μ m and powders of Au^ICl-[P(C₆H₅)₃] (>99.9%, Aldrich), Au^{III}(OH)₃ (Wako), and Au₂^{III}O₃ (Wako) were thoroughly mixed with BN and pressed into a disk of 20 mm in diameter, to make the Au L₃ absorption edge jump to be 1.

The mesoporous TiO₂ sample was synthesized in aqueous solution using dodecylamine [9] given by Professor H. Yoshitake at Yokohama National University. The specific surface area (SA) was 1000 m² g⁻¹ and wormhole-like pore size distributed in narrow range centered at 30 Å. The Au/TiO₂ catalyst was prepared by mixing 1 g of TiO₂ (Degussa P25; anatase 70% and rutile 30%) or mesoporous TiO₂ with 50 ml of aqueous solution of HAu^{III}Cl₄ · 4H₂O (Wako, 1.3 mM) (Table 1a–c). The mixture was stirred at 328 K for 4.5–7 h. The pH of the solution was maintained at 8 by adequately adding NaOH [10]. The powder was filtered and washed several times with de-ionized, distilled water. Dried powders were calcined at 523–673 K in air. The Au/TiO₂ catalyst was also prepared by mixing 1 g of TiO₂ (P25) with 100 ml of aqueous solution of HAuCl₄ · 4H₂O (4.2 or 0.51 mM) by adding 42 or 5.1 mM of urea, respectively. The mixture was stirred at 353 K for

4–16 h in the absence of light [11]. Then, the filtered powder was processed similar to the preparation using NaOH and finally calcined at 573 K in air (Table 1d–g). Thus, the obtained Au/TiO₂ catalysts are denoted “Au/(type of TiO₂)-(alkaline used)-(DP time)-(calcined temperature)”, e.g. Au/P25-urea-16-573.

The Au/TiO₂ sample disks were sealed in on-reaction cell for X-ray measurements purged with dry air or with the mixture of CO (5%) and argon (95%). The window was polyethylene naphthalate film of 16 μ m in thickness (Q51-16, Teijin).

2.2. Characterization

Transmission electron microscope images were measured using field-emission-type TEM (JEM-2010F, JEOL) with an accelerating voltage of 200 kV at the Center of Advanced Materials Analysis, Tokyo Institute of Technology (Dr. A. Genseki). The powder was dispersed in carbon tetrachloride using ultrasonic and mounted on carbon-coated Cu grid.

The X-ray measurements were performed at 290 K at the undulator beamline 37XU of SPring-8 (Sayo, Japan). The storage ring energy was 8.0 GeV operated in top-up mode at the ring current of 99–97 mA. A Si(111) monochromator and Rh-coated mirror were used. The undulator gap value was optimized to maximize the X-ray beam flux at each data point. To stabilize the X-ray beam position on the surface of the sample, a feedback mechanism using MOSTAB (monochromator stabilization) [12] was applied. No position change was detected within the range of 50 μ m throughout the beamtime.

A homemade Rowland-type fluorescence spectrometer was used to analyze Au L α_1 emission equipped with Johansson-type Ge(555) crystal ($d = 0.65321$ Å, Saint Gobain). The detail of the spectrometer was described in Refs. [4,13,14]. An ionization chamber was purged with the mixture of nitrogen (30%) and helium (70%) in front of the sample. The opening of slit θ in front of the ionization chamber was 0.25–0.5 mm (horizontal) \times 0.5–1 mm (vertical). The sample was placed in a plane near horizontal. The plane was tilted by 6° toward the incident X-ray

Table 1
Preparation conditions via deposition-precipitation (DP) method and the property of various Au/TiO₂ samples^a

Entry	Alkaline	TiO ₂	pH	DP reaction temperature (K)	DP reaction time (h)	Calcined temperature (K)	Au loading (wt%) ^b	Average Au particle size (Å)
a	NaOH	mesoporous	8	328	7	523	0.21	87 ± 23
b	NaOH	mesoporous	8	328	4.5	673	0.21	78 ± 30
c	NaOH	P25	8	328	7	673	0.09	32 ± 21
d	urea	P25	3 → 8	353	4	573	7.1	37 ± 10
e	urea	P25	3 → 8	353	16	573	6.8	35 ± 19
f	urea	P25	4 → 8	353	4	573	0.97	29 ± 10
g	urea	P25	4 → 8	353	16	573	0.93	29 ± 18

^a Gold precursor was HAuCl₄ · 4H₂O.

^b Evaluated based on the Au L α_1 emission and Au L₃ absorption edge intensity.

beam and by 7° toward the Ge crystal [4,13,14]. A receiving slit **1** was placed at 100 mm from the sample. The opening was 8 mm(h) \times (0.5–4) mm(v). The sample, Ge(555) crystal, and slit **2** in front of the NaI(Tl) scintillation counter (SC) were controlled on Rowland circle (the radius 220 mm). The opening of slit **2** was 8 mm(h) \times 2 mm(v). The sample and SC were covered with a lead plate housing of 1–3 mm thickness except for the incident X-ray beam entrance and the exit of fluorescence X-rays toward the direction of Ge crystal.

With the excitation energy set to 11943.1 eV, Au $L\alpha_1$ emission ($M_5 \rightarrow L_3$; Bragg angle $\theta_B = 77.700^\circ$) spectra were measured. The scan step was ≈ 0.9 eV and the accumulation time was 60 s for a data point. The fluorescence spectrometer was tuned to each emission energy and the Au L_3 -edge XANES spectra were measured. The scan steps were ≈ 7.5 , ≈ 0.5 , and 2.4 eV in the pre-edge, edge, and post-edge energy regions, respectively. The accumulation time was 40–100 s for a data point. The Au $L\alpha_1$ fluorescence and Au L_3 -edge energy values were calibrated to 9713.3 and 11921.2 eV, respectively, for the spectra of Au metal [15]. The energy positions of the monochromator and the fluorescence spectrometer were reproduced within ± 0.1 and ± 0.2 eV, respectively. Some of the XANES spectra for standard Au samples were also measured in transmission mode at beamline NW10A of Photon Factory Advanced Ring at KEK (Tsukuba, Japan). The obtained data resolution was essentially the same as that measured at beamline 37XU at SPring-8 in the transmission mode.

2.3. XAFS data analysis

The XAFS data analysis was performed using XDAP version 2.2.7 (XAFS Services International) based on works of M. Vaarkamp, H. Linders, and D. Koningsberger. The pre-edge background was approximated by the modified Victoreen function $C_2/E^2 + C_1/E + C_0$. The background of post-edge oscillations was approximated by a smoothing spline function calculated by the following equation for the number of data points N .

$$\sum_{i=1}^N \frac{(\mu x_i - BG_i)^2}{\exp(-0.075k_i^2)} \leq \text{smoothing factor}$$

For Au cluster site models (Ti-top and O-top) supported on anatase-type $\text{TiO}_2(001)$ surface, Au L_3 -edge XANES spectra were theoretically generated using FEFF 8.2 [16] in self-consistent field and full multiple scattering calculation modes. The Hedin–Lundqvist self-energy was used for energy-dependent exchange-correlation potential. The calculated potential was corrected by adding a constant shift to “pure imaginary optical potential”. Because the Au $L\alpha_1$ -selecting XANES was measured under the condition that the energy resolution to detect the X-ray fluorescence (2.9 eV) was smaller than the Γ value of Au L_3 level (5.41 eV) [17], the constant energy shift value was set to negative (–1.0 eV) [4,18].

3. Results

3.1. TEM observation of Au/TiO₂ catalysts

High-resolution TEM images were observed for a series of Au/TiO₂ catalysts (Fig. 1). The average Au particle size and the standard deviation are listed in Table 1. The average Au particle size was in the range 29–37 Å supported on anatase-type TiO₂(c–g) versus relatively greater particles size in the range 78–87 Å supported on mesoporous TiO₂(a,b). The Au particle size distribution was especially narrow (standard deviation 10–19 Å) in the cases of d–g prepared using urea. Observed Au particle sizes (Table 1) were basically consistent with values reported in Refs. [10,11].

The degree of Au loading was reflected as the population of spherical darker dots (Au) dispersed on amorphous TiO₂ (a,b) or anatase-type TiO₂ crystalline (c–g) (Fig. 1). The population of Au dots was smaller when NaOH was used during the DP reaction (a–c). The population of Au dots was greater when urea was used (d–g) and the population seems proportional to the initial concentration of $\text{HAuCl}_4 \cdot 4\text{H}_2\text{O}$: 4.2 mM for Fig. 1d and e and 0.51 mM for Fig. 1f and g. The Au loading amount evaluated based on the Au $L\alpha_1$ emission and Au L_3 edge jump intensity (Table 1) was in accord with the trend of Au nano-particles population detectable in the TEM images.

3.2. X-ray spectroscopy for standard Au compounds

The Au $L\alpha_1$ emission spectra were measured for Au metal and $\text{K}^+[\text{Au}^{\text{I}}(\text{CN})_2]^-$. The Γ values for Au L_3 and M_5 levels are 5.41 [17] and 2.18 eV [19], respectively. Based on the FWHM (full width at the half maximum) value of the Au $L\alpha_1$ peak for Au metal (6.5 eV), the energy resolution of fluorescence spectrometer was estimated to 2.9 eV including the contribution of beamline at 9.7 keV. The chemical shift of Au $L\alpha_1$ emission peaks was –0.2 eV for $\text{K}^+[\text{Au}^{\text{I}}(\text{CN})_2]^-$ compared to that for Au metal (Table 2). Because the shift value was comparable to the reproducibility of energy position of the fluorescence spectrometer, the chemical shift was experimentally checked three times and the shift was reproduced and significant.

By tuning the fluorescence spectrometer to each emission peak top, Au $L\alpha_1$ -selecting Au L_3 -edge XANES spectra were measured for Au metal and $\text{K}^+[\text{Au}^{\text{I}}(\text{CN})_2]^-$ (Fig. 2). Satisfying the condition that the energy resolution to monitor the X-ray fluorescence was smaller than that Γ for Au L_3 level [4,18], absorption edge became steeper and the peaks at 11923.3, 11935.3, 11941.3, and 11948 eV depicted in Fig. 2a and those at 11926.8 and 11948 eV depicted in Fig. 2b were sharper and more resolved compared to the corresponding spectra measured in transmission mode (dotted line).

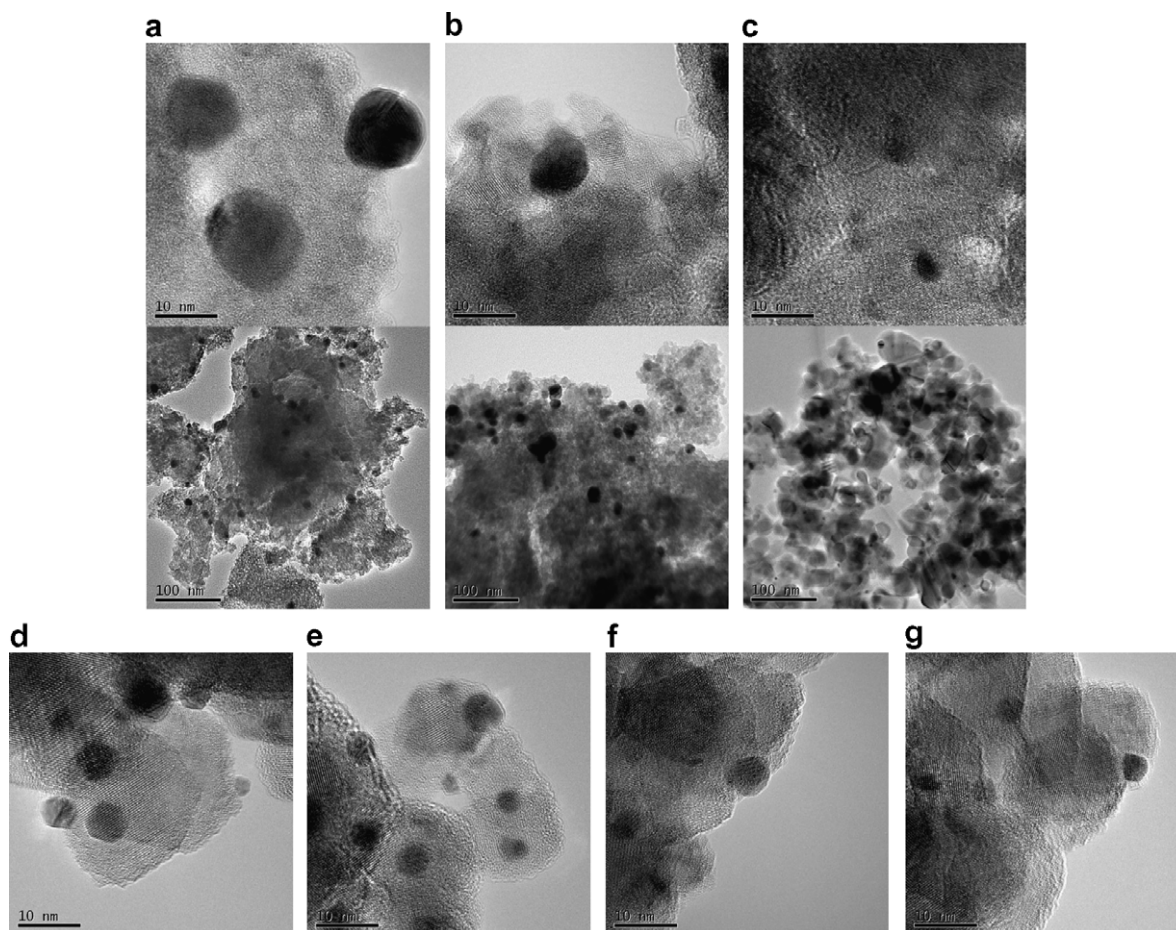


Fig. 1. High-resolution TEM images for Au/TiO₂ catalysts. The images (a–g) correspond to catalyst samples listed in Table 1, entries a–g, respectively.

Table 2

The Au L α_1 emission peak and Au L₃ absorption edge positions for Au standard compounds and Au/TiO₂ catalysts in air or 5% CO by tuning the secondary fluorescence spectrometer to each energy

Sample	Purged gas	Au L α_1 peak energy (eV)	Tune energy (eV)	Au L ₃ edge energy (eV)
Au metal		9713.3	9713.3	11921.2
K ⁺ [Au(CN) ₂] ⁻		9713.1	9713.1	11923.5
AuCl[P(C ₆ H ₅) ₃]				11923.0 ^a
Au/mesoporous–TiO ₂ –NaOH-7-523	air	9713.3	9707.6	11917.1
			9713.0	11920.8
			9718.7	11924.5
Au/mesoporous–TiO ₂ –NaOH-4.5-673	air	9713.4	9713.2	11921.1
Au/P25–NaOH-7-673	air	9713.0	9713.0	11921.1
Au/P25–urea-16-573 (0.93 wt% Au)	air	9713.1	9707.8	11916.5
			9713.1	11921.1
			9718.3	11927.9
			9708.1	11916.4
			9713.4	11921.1
	CO (5%) + Ar (95%)	9713.4	9718.6	11925.0

^a Measured in transmission mode.

3.3. X-ray spectroscopy for Au/TiO₂ catalysts

The Au L α_1 emission spectra for Au/TiO₂ catalysts are depicted in Fig. 3. The peak top energy (9713.3–9713.4 eV) for Au/mesoporous–TiO₂–NaOH-7-523 and Au/mesoporous–TiO₂–NaOH-4.5-673 in air and Au/P25–urea-16-573 (0.93 wt%) in 5% CO was essentially the same

as for Au metal (Table 2). The peak shifted to 9713.0–9713.1 eV for Au/P25–NaOH-7-673 and Au/P25–urea-16-573 both in air. The energy corresponds to the value for K⁺[Au^I(CN)₂]⁻ (Table 2).

Next, the Au L α_1 emission spectra were measured for Au/mesoporous–TiO₂–NaOH-7-523 in air by progressively changing the excitation energy (E_{exc}) on going from

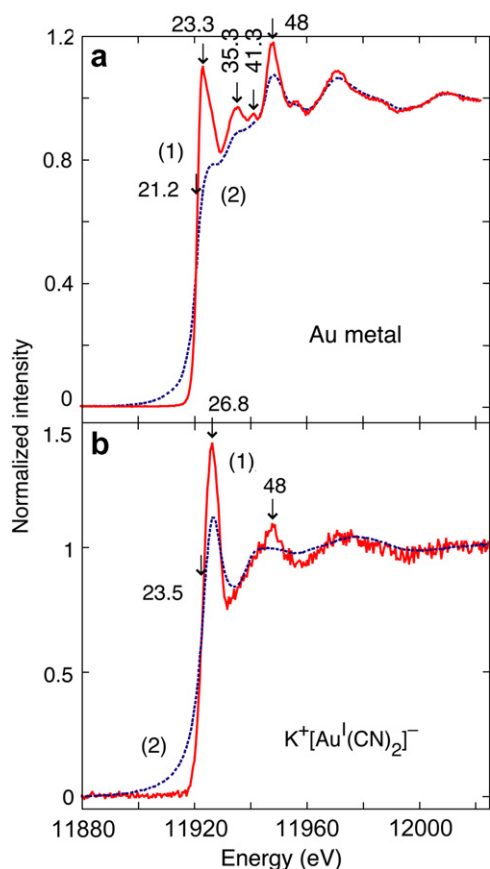


Fig. 2. Au L_3 -edge XANES spectra measured by tuning the fluorescence spectrometer to Au $L\alpha_1$ peak top (solid line, 1) and in transmission mode (dotted line, 2) for Au metal (a) and $K^+[Au^I(CN)_2]^-$ (b).

11943.1 eV to 11919.1 eV [3]. In the E_{exc} range between 11943.1 and 11922.0 eV, the emission peak energy and intensity negligibly changed. When the E_{exc} value decreased to 11919.1 eV, the Au $L\alpha_1$ emission peak shifted to 9711.0 eV and the intensity decreased to 66% [3].

The fluorescence spectrometer was tuned to each peak top (9713.0–9713.4 eV, the arrows in Fig. 3) and Au $L\alpha_1$ -selecting Au L_3 -edge XANES spectra were measured for Au/TiO₂ catalysts listed in Table 1a–c and g. The absorption edge was at 11920.8–11921.1 eV (Table 2) similar to the value for Au metal (11921.2 eV). The sharp, resolved XANES pattern for these Au/TiO₂ catalysts (Fig. 4a-(2), b-(2), and c-(2)) was similar to Au $L\alpha_1$ -selecting XANES for Au metal (Fig. 2a-(1)).

Then, tune energy was set lower than Au $L\alpha_1$ peak top, corresponding to peak intensity of 1/3 (9707.6–9708.1 eV, the arrows in Fig. 3) for Au/mesoporous–TiO₂–NaOH-7-523 in air and Au/P25-urea-16-573 (0.93 wt% Au) in air and in 5% CO. The Au L_3 edge shift compared to the data tuned to Au $L\alpha_1$ peak top was -3.7 eV for Au/mesoporous–TiO₂–NaOH-7-523, smaller than shifts for Au/P25-urea-16-573 in air and in 5% CO (-4.6 to -4.7 eV) (Table 2). The first intense peak at 11923.9–11924.2 eV above absorption edge observed in Fig. 4a-(2), b-(2), and c-(2) became a weak shoulder feature at 11922 eV (Fig. 4a-(1),

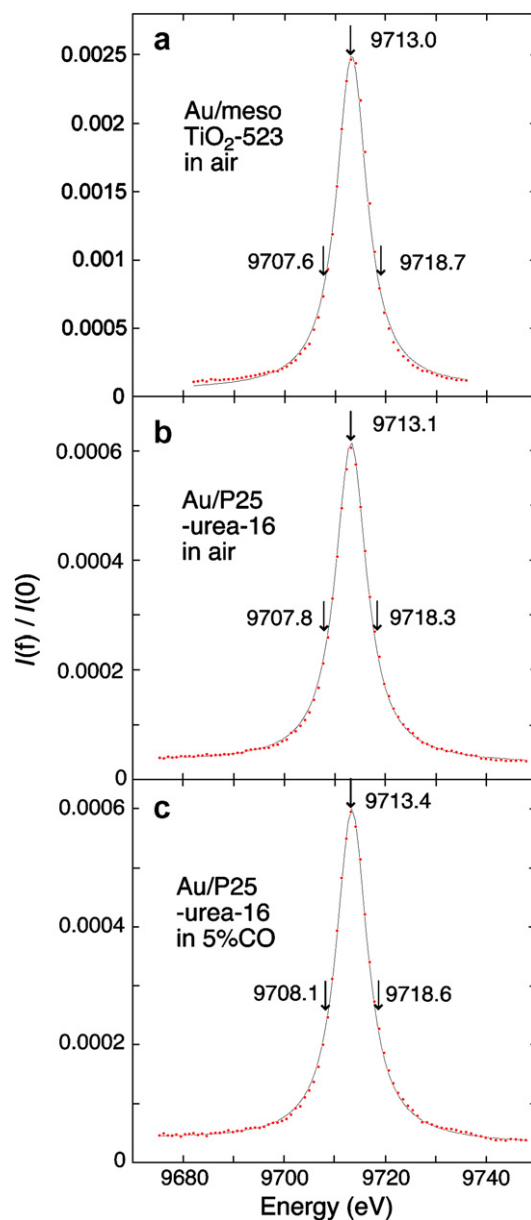


Fig. 3. Au $L\alpha_1$ emission spectra measured for Au/mesoporous–TiO₂–NaOH-7-523 in air (a) and Au/P25–urea-16-573 (0.93 wt% Au) in air (b) and in 5% CO (c). The arrows are tune energy in the Au L_3 -edge XAFS measurements in Fig. 4.

b-(1), and c-(1)). The post-edge pattern looked to shift by -3.7 to -4.7 eV compared to the spectra tuned to Au $L\alpha_1$ peak top.

Subsequently, the fluorescence spectrometer was tuned to the energy corresponding to peak intensity of 1/3, on higher-energy side (9718.3–9718.7 eV, the arrows in Fig. 3). The Au L_3 edge shift compared to the data tuned to Au $L\alpha_1$ peak top was $+6.8$ eV for Au/P25–urea-16-573 in air, greater than shifts for Au/mesoporous–TiO₂–NaOH-7-523 in air and Au/P25–urea-16-573 in 5% CO ($+3.7$ to $+3.9$ eV) (Table 2). The intensity of first intense peak at 11930.0–11931.2 eV above absorption edge was in the order for spectra of Au/P25–urea-16-573 in air

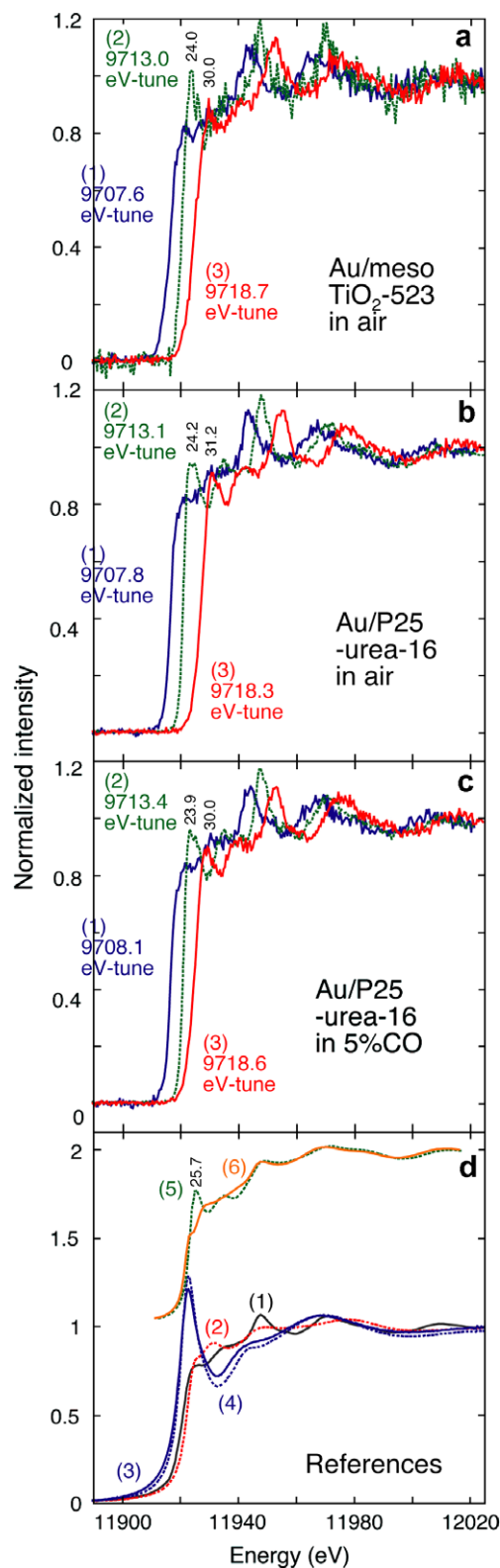


Fig. 4. Au $L\alpha_1$ -selecting XANES spectra measured for Au/mesoporous-TiO₂-NaOH-7-523 in air (a) and Au/P25-urea-16-573 (0.93 wt% Au) in air (b) and in 5% CO (c). Tune energy was 9707.6, 9713.0, and 9718.7 eV (a), 9707.8, 9713.1, and 9718.3 eV (b), and 9708.1, 9713.4, and 9718.6 eV (c). (d) Au L_3 -edge XANES spectra for gold metal (1), Au^I[P(C₆H₅)₃] (2), Au^{III}(OH)₃ (3), Au₂^{III} O₃ (4), and interfacial Au sites located on Ti and O atoms (5 and 6, respectively). 1–4: Experimental, measured in transmission mode. 5, 6: generated for model sites in Fig. 5a (Ti-top) and b (O-top), respectively, using FEFF [16].

(Fig. 4b-(3)) > Au/P25-urea-16-573 in 5% CO (Fig. 4c-(3)) > Au/mesoporous-TiO₂-NaOH-7-523 in air (Fig. 4a-(3)). This resonance peak was reported to be more intense as the Au 5d states were less occupied [20]. The post-edge pattern looked to shift by +3.7 to +6.8 eV compared to the spectra tuned to Au $L\alpha_1$ peak top.

Au $L\alpha_1$ -detecting EXAFS (extended X-ray absorption fine structure) spectra for Au/mesoporous-TiO₂-NaOH-7-523 (0.93 wt%) tuned to 9707.6 and 9718.7 eV (Fig. 3a, arrows) were very similar to each other in the wave-number region 2–9 Å⁻¹ in contrast to the typical difference of state-sensitive spectra in the XANES region (Fig. 4a). A peak due to Au–Au bonding appeared at 2.3 Å (phase shift uncorrected) in the Fourier transform of EXAFS for Au/mesoporous-TiO₂-NaOH-7-523 tuned to 9707.6 and 9718.7 eV and Au/P25-urea-16-573 (0.93 wt% Au) in air tuned to 9713.1 eV (Fig. 3b, arrow), however, a peak due to Au–O bonding [21,22] was unclear/unresolved in the Fourier transform for all the EXAFS spectra.

4. Discussion

State-sensitive Au L_3 -edge XANES spectra tuned to Au $L\alpha_1$ peak (9713.0–9713.4 eV) for Au/TiO₂ catalysts (Fig. 4a-(2), b-(2), and c-(2)) resembled Au $L\alpha_1$ -selecting XANES for Au metal (Fig. 2a-(1)). The Au⁰ state among Au/TiO₂ catalysts was discriminated with this range of tune energy.

When the fluorescence spectrometer was tuned to 9707.6–9708.1 eV, the first intense peak above the edge became a weak shoulder at 11922 eV (Fig. 4a-(1), b-(1), and c-(1)) suggesting greater Au 5d occupation [20,21]. Two types of Au cluster models were considered located either on Ti or on O atom of anatase-type TiO₂(001) surface (Fig. 5a and b, respectively). The spectral pattern, especially in the absorption edge region, was similar to the theoretical XANES generated by FEFF for O-top interfacial Au sites (Figs. 4d-(6) and 5b). The Au L_3 -edge XANES spectra tuned to 9710.4–9710.6 eV for Au/meso-

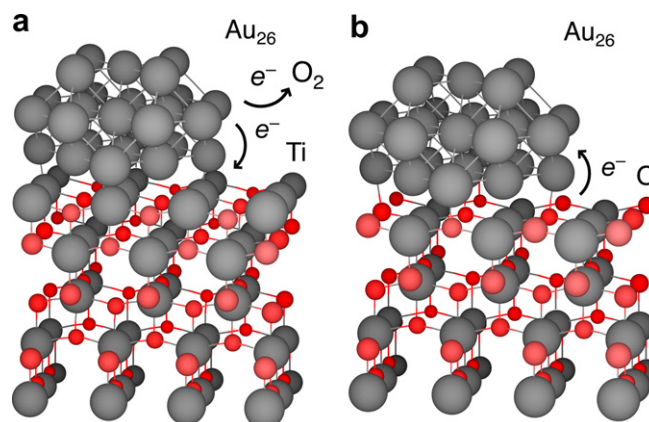


Fig. 5. Au cluster models on anatase-type TiO₂(001) surface terminated with Ti atoms (Ti-top; a) and O atoms (O-top; b).

porous-TiO₂-NaOH-7-523 in air [3] and Au/P25-urea-16-573 (0.93 wt% Au) in 5% CO (not shown) resembled the theoretical data of Fig. 4d-(6) even more. Thus, negative charge transfer from interfacial O atoms to Au is suggested [23–25] at the interface of Au/TiO₂ catalysts, successfully discriminated by tuning the spectrometer to 9707.6–9710.6 eV.

Among the Au L_{α1}-selecting XANES spectra tuned to 9707.6–9708.1 eV, the Au L₃ absorption edge shift compared to XANES spectra tuned to Au L_{α1} peak top was smaller for Au/mesoporous-TiO₂-NaOH-7-523 in air (−3.7 eV) versus −4.6 to −4.7 eV for Au/P25-urea-16-573 in air and in 5% CO (Table 2). This difference can be explained due to the difference of average Au nano-particle size: 87 and 29 Å, respectively. As the Au nano-particle size increases, the effect of charge transfer at the particle-support interface becomes relatively small per Au particle and thus the population of Au⁰ state was greater. Instead, this difference may be explained based on the report that smaller Au particles were relatively more negatively charged [21].

First intense peak above the edge was observed at 11923.9–11924.2 eV by tuning the fluorescence spectrometer to peak top and at 11930.0–11931.2 eV by tuning it to 9718.3–9718.7 eV (Fig. 4). An intense peak appeared at 11925.7 eV for theoretically generated XANES for Ti-top interfacial Au sites (Figs. 4d-(5) and 5a) [24]. Thus, negative charge transfer was suggested from Au 5d to support [22,26] for Au states discriminated by tuning to 9718.3–9718.7 eV. The charge transferred from Au 5d to reduce to Ti³⁺ states at the interface (Fig. 5a).

Among the Au L_{α1}-selecting XANES spectra tuned to 9718.3–9718.7 eV, the Au L₃ absorption edge shift compared to XANES spectra tuned to Au L_{α1} peak top was greater for Au/P25-urea-16-573 in air (+6.8 eV) versus +3.7 to +3.9 eV for the same catalyst in 5% CO and Au/mesoporous-TiO₂-NaOH-7-523 in air. This difference demonstrates that the negative charge transfer from Au to O₂ is only detected for smaller Au particles (mean size 29 Å, Fig. 5a), not for Au/mesoporous-TiO₂-NaOH-7-523 (mean size 87 Å). The Au^I species were detected by Mössbauer and X-ray photoelectron spectroscopy [26] and suggested to be active for CO oxidation. Negative charge transfer from Au to O₂ was supported for Au nano-particle model on rutile-type TiO₂(1 1 0) by ultraviolet photoelectron spectroscopy [27] and density functional theory (DFT) calculations [28]. The effect of O₂ was suggested based on the difference XANES spectrum measured in transmission mode before/after the introduction of O₂ to Au/TiO₂ [20]. The effect of O₂ was *directly* demonstrated by state-sensitive XANES in this work (Fig. 4b-(3)).

The Au^{δ+} site to interact with O₂ may be at the interface based on the similarity of spectral pattern between Fig. 4b-(3) (state-sensitive XANES) and D-5 (theoretical XANES generated for interface Au^{δ+} site model, Fig. 5a), as also proposed based on on-reaction EXAFS measurements [29] and DFT calculations [30].

The pattern of positively-shifted XANES spectra (Fig. 4b-(3)) due to the effects of negative charge transfer from Au to support and/or O₂ was similar to the spectrum for Au metal (Fig. 2A1) shifted by +6.7 eV rather than ones for K⁺[Au^I(CN)₂][−]Au^I (Fig. 2b-(1)), Au^ICl[P-(C₆H₅)₃], Au^{III}(OH)₃, or Au₂^{III}O₃ (Fig. 4d-(2)–(4)). Thus, the Au states discriminated by tuning the spectrometer to 9718.3 eV for Au/P25-urea-16-573 in air were for electron-deficient Au nano-particle sites.

Acknowledgements

This work was supported from the Grant-in-Aid for Scientific Research (Y.I., C17550073) and the Research Foundation for Opto-Science and Technology (Y.I. 2005–2006). The X-ray measurements were performed under the approvals of the SPring-8 Program Review Committee (2006A1156 and 2006B1486) and Photon Factory Proposal Review Committee (2005G220).

References

- [1] A. Cho, *Science* 299 (2003) 1684.
- [2] A.T. Bell, *Science* 299 (2003) 1688.
- [3] Y. Izumi, D. Masih, J.P. Candy, H. Yoshitake, Y. Terada, H. Tanida, T. Uruga, X-ray absorption fine structure 13th international conference, in: B. Hedman, P. Pianetta, (Eds.), *AIP Conference Proceedings* 882 (2007) 588–590.
- [4] Y. Izumi, H. Nagamori, T. Kiyotaki, D. Masih, T. Minato, E. Roisin, J.P. Candy, H. Tanida, T. Uruga, *Anal. Chem.* 77 (21) (2005) 6969.
- [5] Y. Izumi, H. Nagamori, *Bull. Chem. Soc. Jpn.* 73 (2000) 1581.
- [6] K. Hämäläinen, D.P. Siddons, J.B. Hastings, L.E. Berman, *Phys. Rev. Lett.* 67 (1991) 2850.
- [7] F.W.F. de Groot, *Top. Catal.* 10 (2000) 179.
- [8] Y. Izumi, T. Kiyotaki, T. Minato, Y. Seida, *Anal. Chem.* 74 (15) (2002) 3819.
- [9] H. Yoshitake, T. Sugihara, T. Tatsumi, *Chem. Mater.* 14 (3) (2002) 1023.
- [10] G.R. Bamwenda, S. Tsubota, T. Nakamura, M. Haruta, *Catal. Lett.* 44 (1997) 83.
- [11] R. Zanella, L. Delannoy, C. Louis, *Appl. Catal. A* 291 (2005) 62.
- [12] A. Krolzig, G. Materlik, M. Swars, J. Zegenhagen, *Nucl. Instr. Meth.* 219 (2) (1984) 430.
- [13] Y. Izumi, F. Kiyotaki, H. Nagamori, T. Minato, *J. Electro. Spectro. Relat. Phenom.* 119 (2/3) (2001) 193.
- [14] Y. Izumi, H. Oyanagi, H. Nagamori, *Bull. Chem. Soc. Jpn.* 73 (9) (2000) 2017.
- [15] J.A. Bearden, *Rev. Mod. Phys.* 39 (1967) 78.
- [16] A.L. Ankudinov, B. Ravel, J.J. Rehr, S.D. Conradson, *Phys. Rev. B* 58 (1998) 7565.
- [17] M.O. Krause, J.H. Oliver, *J. Phys. Chem. Ref. Data* 10 (1979) 329.
- [18] Y. Izumi, D. Masih, E. Roisin, J.P. Candy, H. Tanida, T. Uruga, *Mater. Lett.* 61 (2007) 3833.
- [19] G. Zschornack, *Handbook of X-ray data*, Springer, Berlin-Heidelberg, 2007.
- [20] N. Weiher, A.M. Beesley, N. Tsapatsaris, L. Delannoy, C. Louis, J.A. van Bokhoven, S.L.M. Schroeder, *J. Am. Chem. Soc.* 129 (8) (2007) 2240.
- [21] J.T. Miller, A.J. Kropf, Y. Zha, J.R. Regalbutto, L. Delannoy, C. Louis, E. Bus, J.A. van Bokhoven, *J. Catal.* 240 (2006) 222.
- [22] E.D. Park, J.S. Lee, *J. Catal.* 186 (1999) 1.
- [23] D.B. Akokekar, G. Foran, S.K. Bhargava, *J. Synchrotron Radiat.* 11 (2004) 284.
- [24] M.S. Chen, D.W. Goodman, *Science* 306 (2004) 252.

- [25] D.W. Goodman, *Catal. Lett.* 99 (1–2) (2005) 1.
- [26] D. Boyd, S. Golunski, G.R. Hearne, T. Magadzu, K. Mallick, M.C. Raphulu, A. Venugopal, M.S. Scurrall, *Appl. Catal. A* 292 (2005) 76.
- [27] T. Okazawa, M. Kohyama, Y. Kido, *Surf. Sci.* 600 (2006) 4430.
- [28] L.M. Molina, M.D. Rasmussen, B. Hammer, *J. Chem. Phys.* 120 (16) (2004) 7673.
- [29] S.H. Overbury, V. Schwartz, D.R. Mullins, W. Yan, S. Dai, *J. Catal.* 241 (2006) 56.
- [30] L.M. Molina, B. Hammer, *Appl. Catal. A* 291 (2005) 21.